Carbohydrate Polymers 93 (2013) 240–245

Contents lists available at SciVerse ScienceDirect

Carbohydrate Polymers

journal homepage: www.elsevier.com/locate/carbpol

AFM characterization of spin coated carboxylated polystyrene nanospheres/xyloglucan layers on mica and silicon

Adriana F. Lubambo[a,b,*], Neoli Lucyszyn[b,d], Cesar L. Petzhold[c], Maria-R. Sierakowski[b], Wido H. Schreiner[a], Cyro K. Saul[a]

[a] Department of Physics, Universidade Federal do Paraná-UFPR, Centro Politécnico, P.O. Box 19044, Curitiba, Brazil
[b] Department of Chemistry, Universidade Federal do Paraná-UFPR, Centro Politécnico, P.O. Box 19081, Curitiba, Brazil
[c] Department of Organic Chemistry, Universidade Federal do Rio Grande do Sul – UFRGS, Campus do Vale, P.O. Box 15003, Porto Alegre, Brazil
[d] School of Education and Humanities, Pontifícia Universidade Católica do Paraná – PUCPR, Campus Curitiba, Brazil

ARTICLE INFO

Article history:
Received 8 February 2012
Received in revised form 12 July 2012
Accepted 31 July 2012
Available online 11 August 2012

Keywords:
Organic thin films
Mixtures
Self-assembly
Nanosphere arrays
Spin coating
Xyloglucan
Carboxylated polystyrene

ABSTRACT

Self-assembled nano-arrays have a potential application as solid-phase diagnostics in many biomedical devices. The easiness of its production is directly connected to manufacture cost reduction. In this work, we present self-assembled structures starting from spin coated thin films of carboxylated polystyrene (PSC) and xyloglucan (XG) mixtures on both mica and silicon substrates. AFM images showed PSC nanospheres on top of a homogeneous layer of XG, for both substrates. The average nanosphere diameter fluctuated for a constant speed and it was likely to be independent of the component proportions on the mixture within a range of 30–50% (v/v) PSC. It was also observed that the largest diameters were found at the center of the sample and the smallest at the border. The detected nanospheres were also more numerous at the border. This behavior presents a similarity to spin coated colloidal dispersions. We observed that the average nanosphere diameter on mica substrates was bigger than the nanosphere diameters obtained on top of silicon substrates, under the same conditions. This result seems to be possibly connected to different mixture–surface interactions.

1. Introduction

Multi-component arrays having small features, preferentially at the nanoscale, are of special importance for several applications like: investigation of single molecule interactions (Powell, Tran, Kim, & Yoon, 2009); biochips (Wadhwa, 1990); and biologically integrated electronic devices (Haddon and Lamola, 1985). Nowadays, there is a growing need for point-of-care diagnostics kits for infectious diseases, which preferentially have to present the following characteristics: have low cost; be easy to design; present high-throughput; avoid complex procedures and equipments; and be able to generate reliable results (high signal to noise ratio) (Hauck, Giri, Gao, & Chan, 2010). One of the simplest ways to address this issue can be the nanoscale self-assembly driven patterned thin films (Blawas & Reichert, 1998; Rusmini, Zhong, & Feijen, 2007). This method provides some advantages like, simplicity, fast production, and effortlessness, when compared to top-down approaches. Besides these advantages there is also the consequent low cost.

Another important point related to this area is protein immobilization, where it is of crucial importance to maintain protein functionality, while studying protein/protein, bio-molecule/protein, or even to detect antibody/antigen events on a solid patterned support (Powell et al., 2009). Thus, the ability to spatially direct the immobilization and preserving the molecule functionality are key issues to succeed in having a high resolution and sensitive device.

One way of producing such devices is the use of mixtures from synthetic and natural materials as in bioblends (Biresaw, Carriere, & Willett, 2004). It allows the production of materials with new emergent properties, which are otherwise absent when the single components are used separately. Besides the fact that one of the components is natural and abundant, the addition of a synthetic one may produce, as one of the advantages, an acceptable water-resistance blend while maintaining biocompatibility (Biresaw et al., 2004), as in synthetic polymer/polysaccharides blends.

In a previous work (Lubambo et al., 2011), we have shown that it is possible to obtain arranged self-assembled arrays of both polystyrene and xyloglucan depending of the concentration of each component in the original mixture. In this work, self-assembled nanostructures were obtained by spin coating xyloglucan/carboxylated polystyrene mixtures and deposited it on

* Corresponding author at: UFPR, Av. Cel. Francisco H. dos Santos, Centro Politécnico, Jardim das Américas, 81531-990 Curitiba-PR, Brazil. Tel.: +55 41 33613092; fax: +55 41 33613418.
E-mail addresses: af.lubambo@uol.com.br, af.lubambo@gmail.com (A.F. Lubambo).

0144-8617/$ – see front matter © 2012 Elsevier Ltd. All rights reserved.
http://dx.doi.org/10.1016/j.carbpol.2012.07.084

both mica and silicon substrates. The resulting nanostructured thin films were investigated using AFM and XPS.

Xyloglucan is a neutral, branched polysaccharide found in the primary cell walls of non-graminaceous (monocotyledons), as well as in the cotyledon of some dicotyledonous seeds. Its chemical structure has a cellulose-like backbone, composed of β-glucosyl ring units with ribbon-like conformation, where single-unit of xylose and galactose substituents are part of the branches (Hayashi, 1989). This biopolymer, like many other polysaccharides, is potentially important for commercial and medical applications. In the food industry it can be used as a texture modifier and in the medical field it can acts as a drug release controller (Bhattacharya, Bal, Mukherjee, & Bhattacharya, 1991; Jo, Petri, Beltramini, Lucyszyn, & Sierakowski, 2010; Miyazaki et al., 1998; Miyazaki, Kawasaki, Kubo, Endo, & Attwood, 2001).

Polystyrene is a well-known and studied synthetic polymer which when blended to biopolymers reduces its degradation rates. However, due to its low hydrophilicity, the blending with biopolymers generally segregates. Thus, we have used an asymmetric triblock copolymer PS-b-PAA-b-PS, having a very short polar PAA segment to induce a better interaction with XG biopolymer. These strategies open many possible applications in tissue engineering and drug release control (Leung et al., 2009).

2. Materials and methods

2.1. Polysaccharide

Branched neutral polysaccharide xyloglucan (XG), M_w of 843,000 g/mol was extracted from the seeds of *Guibourtia hymenifolia*. The XG (54.2% yield, w/w) is formed by glc:xyl:gal molar ratio of 3.3:2.3:1.0, respectively (Lucyszyn et al., 2011). After extraction, XG was filtered under pressure through cellulose acetate membranes with 0.22 μm pore diameters (Millipore®) and precipitated with ethanol to obtain purified XG polysaccharide before use.

2.2. Triblock copolymer PS-b-PAA-b-PS

A triblock copolymer, which from now on, for sake of simplicity, will be treated as carboxylated polystyrene (PSC), M_w of 40,073 g/mol; $M_w/M_n = 1.3$, acid value of 25.41 mg KOH/g used in this investigation was prepared by PS-b-PAA-b-PS synthesis. Initially a macro chain transfer agent of polystyrene (MTA-PS) was prepared by RAFT polymerization. Styrene monomer (0.048 mol) was polymerized in bulk at 110 °C using DBTTC (dibenzyltrithiocarbonate) (5.0×10^{-5} mol) as a chain transfer agent. After 24 h the reaction was completed and the polymer was precipitated in ethanol and dried under vacuum. For the preparation of the triblock copolymer, acrylic acid was polymerized in anisole at 110 °C for 24 h using MAT-PS and AIBN as radical initiator. The final product was precipitated in ethanol, dried under vacuum and characterized by SEC. The amount of incorporated acrylic acid was determined by titration (AOCS, 1980). The content of each polymer block was determined by ^{1}H NMR (300 MHz, Varian) corresponding to a PS_{181}-b-PAA_{18}-b-PS_{181}.

2.3. Substrates

Grade V-4 mica muscovite substrate obtained from SPI supplies® was cleaved using a scotch tape and immediately used for adsorption experiments. Commercial boron-doped, 450 μm-thick, (1 1 1) orientation silicon wafers were used as solid substrates. The substrates were cleaved into 1 cm^2 pieces with a diamond-tipped scriber. After cleavage, the substrates were cleaned, prior to polysaccharide deposition, in a boiling solution as described in Hirose, Yasaka, Takakura, and Miyazaki (1991), preserving the SiO_2 oxide layer and maintaining the surface hydrophilicity. Ultra-pure water (Millipore, Milli-Q, 18.2 MΩ cm) was used in the cleaning solution and for abundantly rinsing the silicon surface, after the cleaning process.

Table 1
Tested mixture proportions.

Sample proportion XG/PSC% (v/v)	XG (15 mg/L)	
	PSC (30 mg/L)	PSC (60 mg/L)
95/05	X	
90/10	X	
85/15	X	X
80/20	X	X
75/25	X	
70/30	X	X
65/35	X	
60/40	X	
55/45	X	
50/50	X	

2.4. Adsorption protocols for model surfaces

Xyloglucan mother solution was prepared with 1.5 mg of polysaccharide dissolved in 100 mL of Milli-Q water and stirred during 24 h. Carboxylated polystyrene mother solutions were prepared with two different concentrations 3.0 and 6.0 mg in 100 mL chloroform with the goal to produce PSC nanospheres on top of a xyloglucan layer. The mixtures were prepared by blending different proportions of XG stock solution with PSC stock solution to a final volume of 1 mL, according to Table 1.

The mixtures were prepared by stirring the solutions during 1 min in a vortex mixer, prior to the spin coating deposition. A mixture drop (20 μL) was immediately pipetted onto the center of a mica substrate, which was rotating at 1000 rpm and kept at the same condition during 1 min. The substrate was then accelerated to 2000 rpm and it was kept at this speed for 30 s to eliminate solution excess. The sample was not rinsed during spinning. After deposition, the samples were kept in a controlled chamber during 24 h, at 24 °C and 45% relative humidity, before analysis.

2.5. Atomic force microscopy measurements

AFM imaging was performed using a commercial Shimadzu SPM-9500J3 microscope at room temperature (~24 °C). Images were taken in dynamic tapping mode (TM-AFM) with an oxide-sharpened micro-fabricated silicon cantilever (μ-Masch), whose nominal spring constant was 4.7 N/m and tip radius of curvature less than 10 nm. The scanning rate was 1 Hz and the image resolution was 256 × 256 pixels. The operating point was adjusted to minimize the interaction between tip and sample and to avoid soft layer deformation. After acquisition, image treatment was performed using Shimadzu software for flattening. Grain analysis was performed using threshold detection and histograms were carried out using SPIP V.4.3.4.0. The image background was noise filtered whenever needed prior to contour detection.

2.6. X-ray photoelectron spectroscopy measurements

XPS analyses were performed with an ESCA 3000 VG Microtech photoelectron spectrometer. Aluminum K_α radiation was used and high resolution spectra were taken with 20 eV pass energy. The vacuum in the sample chamber during measurements was about 10^{-9} mbar. Charging effects were corrected using the K $2p_{3/2}$ line (292.80 eV) for mica as a reference (Bhattacharyya, 1989; Dufrêne, Marchal, & Rouxhet, 1999; Liu & Brown, 1998). Data treatment was

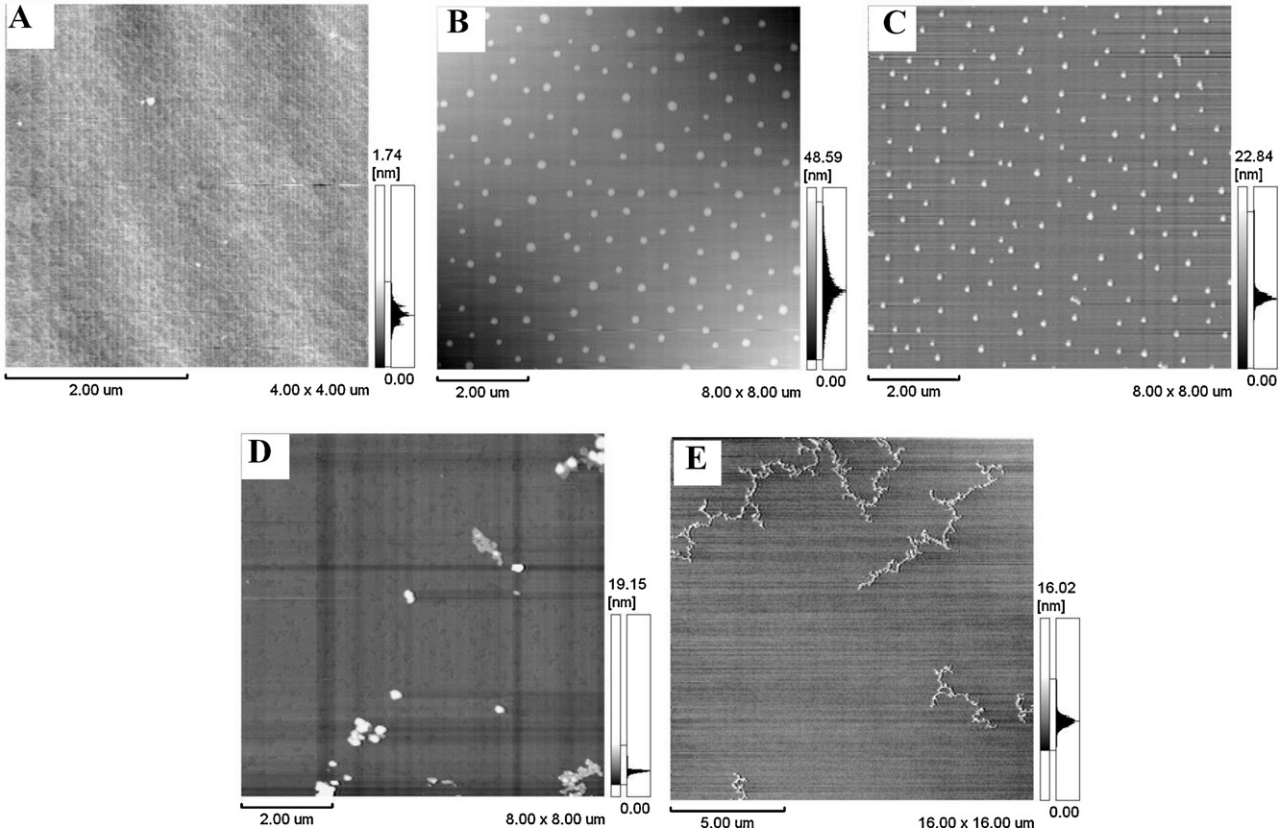

Fig. 1. Dynamic mode AFM images. (A) XG/PSC (90/10%, v/v) sample (4 μm × 4 μm). (B) XG/PSC (65/35%, v/v) sample, showing PSC nanospheres on a XG matrix (8 μm × 8 μm). (C) XG/PSC (50/50%, v/v) (8 μm × 8 μm). (D) Sample with 100% PSC (8.0 μm × 8.0 μm). (E) Sample with 100% XG (16 μm × 16 μm).

carried out using XISDP32V.3 from XPS International© software. Shirley background was used for subtraction.

3. Results and discussion

3.1. Morphological analysis on mica

3.1.1. XG (15 mg/L) and PSC (30 mg/L)

Dynamic mode AFM images of XG/PSC thin films on mica revealed different morphologies as a function of XG/PSC proportions in the mixture, as shown in Fig. 1. At PSC concentration from 5% to about 15% (v/v) PSC, nanosphere arrays were not observed, as seen in Fig. 1A, for 10% (v/v) PSC. For PSC concentrations from 20% to about 30% (v/v), the assembly and the structure of the nanospheres array became non-reproducible. Finally, for higher concentrations, from 35% to about 50% (v/v) PSC, nanosphere arrays were observed on top of a homogeneous background layer, as seen in Fig. 1B and C, for 35% and 50% (v/v) PSC, respectively.

It is worthwhile to point out that for pure XG aqueous solution and pure PS chloroform solution the dried thin films present completely different morphologies compared to the mixed solutions, as shown in Fig. 1D and E, respectively. There is a large number of reports dealing with the orientation of block copolymers in thin film formation and many investigators have studied its effects on the final morphology and structures of the imposed interfaces (Bucknall, 2004; Cacicchi, Berthiaume, & Russel, 2005; Priestley, Ellison, Broadbelt, & Torkelson, 2005; Chen, Gong, Huang, & He, 2007; Sordi, Riegel, Ceschi, Müller, & Petzhold, 2010). The morphology in a thin film, supported by a substrate, is the result of specific interactions between polymer, air and substrate. The difference in surface energies of both blocks polystyrene and poly(acrylic acid) governs the relative wettability, as one block (PAA) wets the substrate and the other (PS) wets the air interface. In the case of PS-b-PAA-b-PS triblock thin films large aggregates were observed, as in Fig. 1D, since the molar composition of PAA is very low (<5 mol%) and it should be attached to the substrate. Xyloglucan is a neutral branched polysaccharide with flexible random coil conformation, it tends to aggregate even at very low solution concentration (Lucyszyn et al., 2011). As a hydrophilic polymer it wets hydrophilic substrates like mica substrate and forms an entangled nanoporous network of branched fibrous structures as seen in Lubambo et al. (2009) and Fig. 1E.

Similar features found in pure XG/water and PSC/chloroform system on mica could be expected and would be governed by surface energy minimization in a two phase mixture XG/PSC deposited on high energy surfaces like mica and silicon. In this mixed system of PSC/XG, since the triblock copolymer has lower surface energy than that of XG, after the deposition, the triblock would be on the top layer. Therefore, it is reasonable to expect that the nanospheres, seen in Fig. 1B and C, are composed of PSC. Furthermore, XG with higher surface energy than PSC would form an entangled nanoporous network. It would be preferentially wetting the solid surfaces (mica, silicon) and anchoring the PSC nanospheres. The nanosphere PSC composition was confirmed by XPS, as seen in Section 3.3.

Average nanospheres diameter D and standard deviation δD measured at the sample substrate center, as a function of PSC proportion in the mixture is shown in Table 2. The fluctuation observed in PSC nanoparticles diameter does not seem to show a correlation with the XG/PSC mixture proportion. In fact, if we simplify the spin coating dynamics of this system, assuming the balance between centrifugal and viscous forces, the process selects the diameter as a

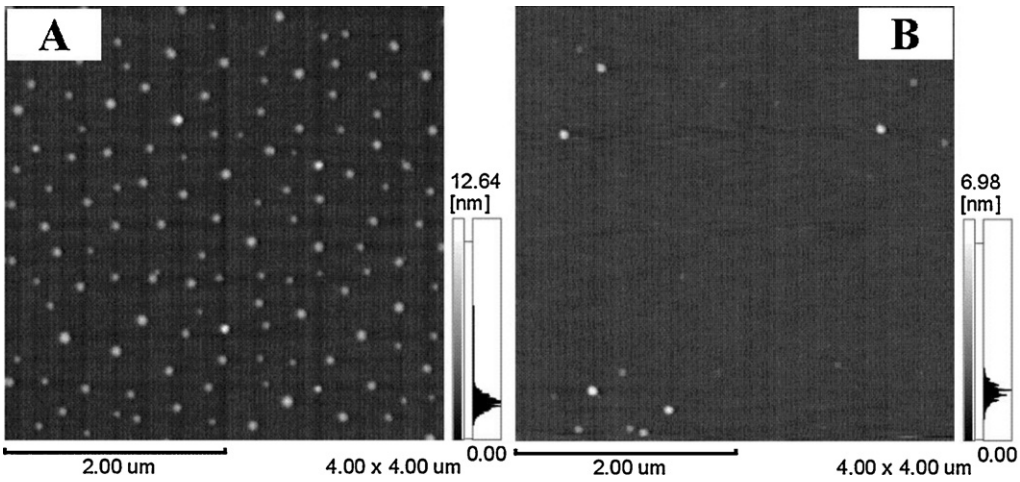

Fig. 2. Dynamic mode AFM images. (A) Sample with XG/PSC (70/30%, v/v), showing PSC nanospheres on a XG layer (4 μm × 4 μm). (B) XG/PSC (70/30%, v/v) sample, after selective dissolution with chloroform (4 μm × 4 μm).

function of angular velocity of the chuck (Lubambo et al., 2011). If this assumption holds, the nanosphere diameter will decrease from the center to the border of the sample. Table 3 shows the average nanosphere diameter measured as a function of the distance from the center at regular steps, for sample XG/PSC (65/35%, v/v). As can be noticed, the average diameter is higher at the sample center, $D^* = 129$ nm and reaches the minimum value, $D^* = 56$ nm at the border, confirming thus, our assumption.

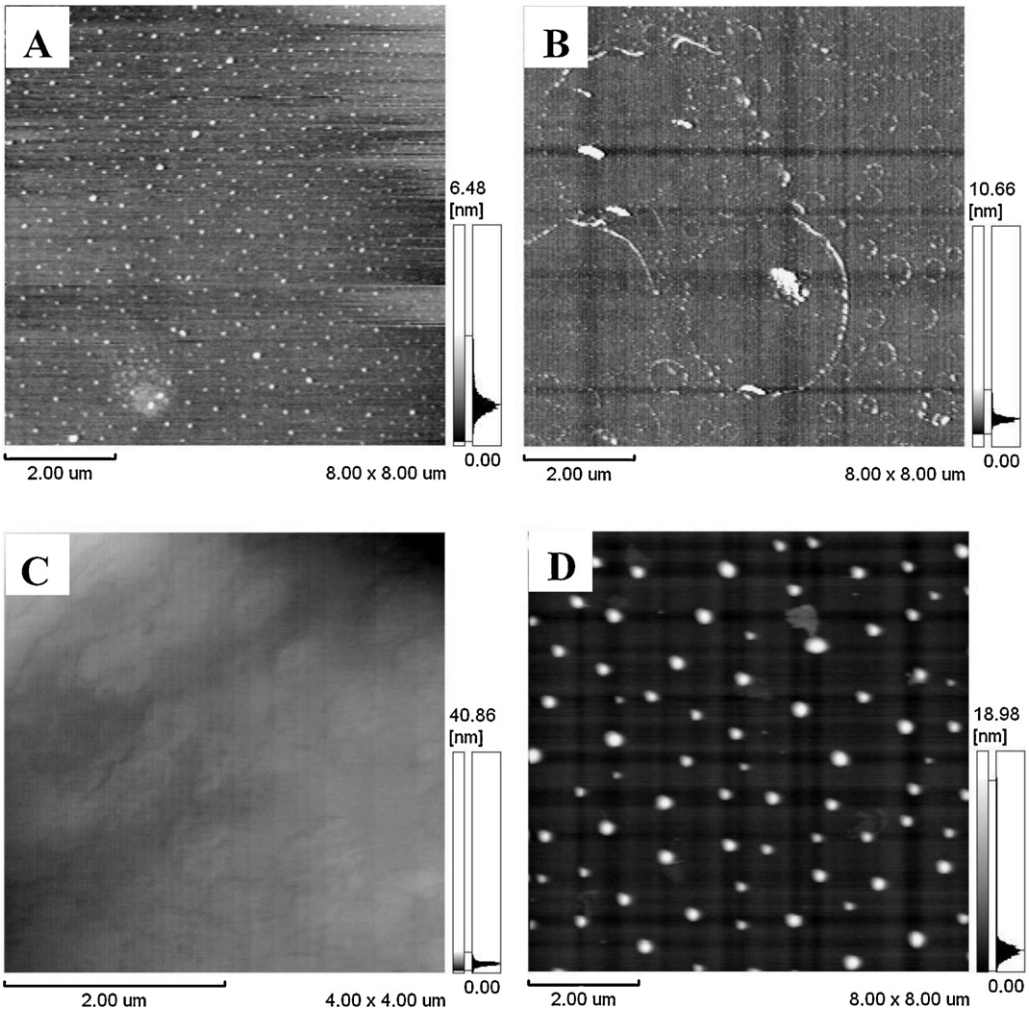

Fig. 3. Dynamic mode AFM images. (A) Sample with XG/PSC (70/30%, v/v) sample, showing PSC nanospheres on a XG layer on silicon, (8 μm × 8 μm). (B) XG/PSC (70/30%, v/v) sample, after first step selective dissolution with chloroform (8 μm × 8 μm). (C) XG/PSC (70/30%, v/v) sample, after second step selective dissolution with chloroform (4 μm × 4 μm). (D) XG/PSC (70/30%, v/v) sample, showing PSC nanospheres on a XG layer on mica (8 μm × 8 μm).

Table 2
Average diameter (D) and standard deviation (δD) of the measured nanospheres as a function of XG and PSC concentration in mixture, as well as its tip deconvoluted correspondents (D^*).

XG/PSC proportion % (v/v)	$D \pm \delta D$ (nm)	D^* (nm)
70/30	185 ± 36.9	73
65/35	162 ± 22.8	61
60/40	158 ± 37.1	59
55/45	96 ± 15.1	28
50/50	108 ± 12.8	34

Measured diameter: D (nm) and standard deviation: δD (nm), tip deconvoluted diameter: D^* (nm).

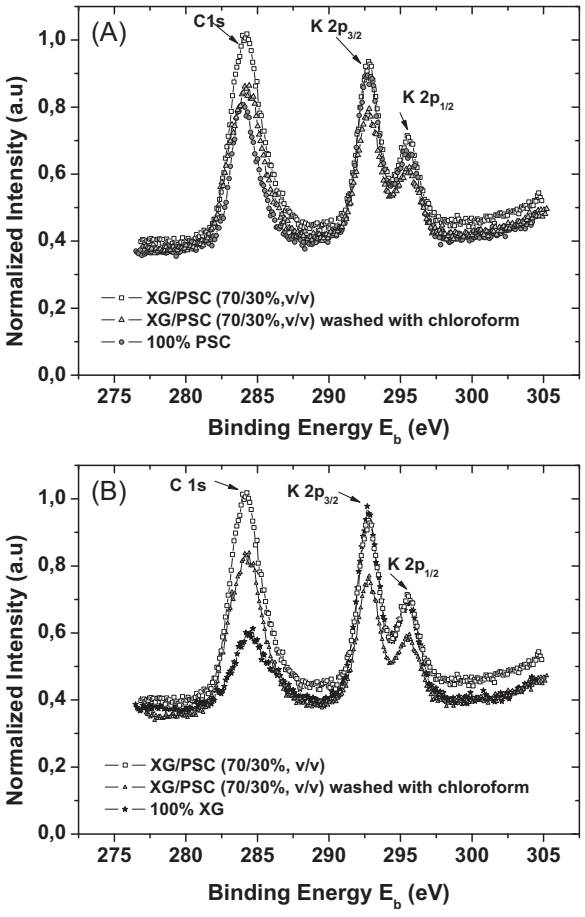

Fig. 4. For XG stock solution concentration $XG_c = 15$ mg/L and $PSC_c = 60$ mg/L. (A) XPS C1s and K $2p_{3/2}$ and K $2p_{1/2}$ spectra of the XG/PSC (70/30%, v/v) sample, the same sample after selective dissolution with chloroform and 100% PSC for integrated intensity comparison. (B) XPS C1s and K $2p_{3/2}$ and K $2p_{1/2}$ spectra of the XG/PSC (70/30%, v/v) sample, the same sample after selective dissolution with chloroform and 100% XG for integrated intensity comparison.

It is important to notice that the number of nanospheres detected increases reaching a maximum value at the border. Theoretical simulations for colloidal systems, under centrifugal and viscous forces, confirm the same results (Zhao & Marshall, 2008).

3.1.2. XG (15 mg/L) and PSC (60 mg/L)

At the proportion XG/PSC (70/30%, v/v) tested, a nanosphere array was produced whose measured average diameter was $D = 152 \pm 32$ nm, shown in Fig. 2A. A selective washing with chloroform was performed to test the nanosphere composition in one step. Two chloroform drops of 20 μL were pipetted, and the excess was eliminated by capillarity. Then, the sample was left to dry 24 h before imaging. After washing, the assembled pattern of nanospheres disappeared as well as it was noticed the presence of a few remaining aggregates, as shown in Fig. 2B.

3.2. Morphological analysis on silicon

3.2.1. XG (15 mg/L) and PSC (30 mg/L)

This mother solution concentration, already tested for mica, was also tried on silicon for two reasons: to observe if eventual changes in substrates could influence the array formation and because silicon can be micro-machined and, therefore, it could be suitable for biosensors purposes. The nanosphere array was formed, as it can be seen, in Fig. 3A, however the average diameter measured was $D = 81.3 \pm 18$ nm, which is smaller when compared to the same conditions on mica, $D = 185 \pm 36.9$ nm and it is possible to observe differences in array organization. These morphology features can be possibly explained by differences in substrate–mixture interactions, linked to the friction coefficient produced by the mixture flow on the interface (Brochard-Wyart, de Gennes, Hervert, & Redon, 1994). On mica, this result suggests that, the friction coefficient should be larger, thus mixture–substrate interaction is more significant than on silicon.

Selective washing with chloroform was again performed to test the nanosphere composition using the same procedure explained before. This procedure generated the exact same results as before, the presence of aggregates, as shown in Fig. 3B, indicating that the nanospheres are composed of PSC. Repeating the procedure, it is possible to observe that only a homogeneous XG layer was left.

3.3. X-ray photoelectron spectroscopy

XPS analysis from C1s photoelectron peak intensity for sample XG/PSC (70/30%, v/v) and the same sample after washing with chloroform show a decay of intensity as seen in Fig. 4A and B. This decay clearly indicates material removal. Furthermore, looking at the two spectra (before and after washing), it is possible to remark that this C1s decay in peak intensity, Fig. 4A, is located exactly at the area corresponding to the characteristic energy of polystyrene signature (benzene ring, $E_b = 284.66$ eV) (Beamson & Briggs, 1992). Thus, this experimental evidence shows that the nanospheres withdrawn by washing, seen in Fig. 2B are composed of PSC and the remaining bottom layer is composed of XG.

Table 3
Average diameter (D), minimum measured diameter (D_{min}) standard deviation (δD) of the measured nanospheres as a function of the sample center distance, as well as its tip deconvoluted correspondents (D^*).

Measurement on the sample	Number of detected spheres	Minimum diameter measured, D_{min} (nm)	$D \pm \delta D$ (nm)	D^* (nm)
1-Center	19	180	298 ± 47	129
2	27	158	239 ± 52	100
3	45	120	190 ± 30	75
4-Border	76	94	151 ± 17	56

Measured diameter: D (nm) and standard deviation: δD (nm), tip deconvoluted diameter: D^* (nm).

4. Conclusion

Carboxylated polystyrene nanosphere arrays on top of a xyloglucan layer were produced for both mica and silicon by spin coating. On mica, the nanosphere average diameter does not depend on (XG/PSC) proportions in the mixture within the concentration range tested, between 30% and 50% (v/v) of PSC. It indicates to be dependent of the angular speed of the chuck. This assumption is confirmed experimentally by the decrease of the average diameter as a function of the distance from the center of the sample: the higher average diameter being found on the center of the sample and the lower at the border. The number of nanospheres detected is also higher at the border. This behavior is similar to spin coated colloidal dispersions. When the average nanospheres diameter of carboxylated polystyrene array on silicon is compared to the array formed on mica, at the same conditions, it is found to be much smaller. This difference can be explained by differences in substrate–mixture interaction. On mica, the interaction should be larger, allowing preferentially the washing away of smaller nanospheres diameters from the substrate. It was also visually observed that the distances between the nanospheres on top silicon are smaller than on top of mica, but not organized as well.

Acknowledgments

The authors acknowledge the INCT for Diagnostics in Public Health/CNPQ, CAPES (RedeNanobiotec) and CNPq for funding and BIOPOL/UFPR, MFA/UFPR and LITS/UFPR for material support.

References

AOCS. (1980). *Official methods and recommended practices of the American Oil Chemists' Society* (3rd ed.). Champaign: AOCS Press. (official method Te 2a-64).

Beamson, G., & Briggs, D. (1992). *High resolution XPS of organic polymers, the scienta ESCA300 database*. Chichester: John Wiley & sons., p. 74.

Bhattacharyya, K. G. (1989). Adsorption of carbon dioxide on mica surfaces. *Langmuir*, *5*(5), 1155–1162.

Bhattacharya, S., Bal, S., Mukherjee, R. K., & Bhattacharya, S. J. (1991). Rheological behavior of tamarind (*Tamarindus indica*) kernel powder (TKP) suspension. *Journal of Food Engineering*, *13*, 151–158.

Biresaw, G., Carriere, C. J., & Willett, J. L. (2004). Interfacial adhesion in model bioblends. *Journal of Applied Polymer Science*, *94*(1), 65–73.

Blawas, A. S., & Reichert, W. M. (1998). Protein patterning. *Biomaterials*, *19*(7–9), 595–609.

Brochard-Wyart, F., de Gennes, P.-G., Hervert, H., & Redon, C. (1994). Wetting and slippage of polymer melts on semi-ideal surfaces. *Langmuir*, *10*, 1566–1572.

Bucknall, D. G. (2004). Influence of interfaces on thin polymer film behavior. *Progress in Materials Science*, *49*(5), 713–786.

Cacicchi, K. A., Berthiaume, K. J., & Russel, T. P. (2005). Solvent annealing thin films of poly(isoprene-b-lactide). *Polymer*, *46*(25), 11635–11639.

Chen, D., Gong, Y., Huang, H., & He, T. (2007). Competition of lamellar orientation in thin films of a symmetric poly(styrene)-b-poly(L-lactide) diblock copolymer in melt state. *Macromolecules*, *40*(18), 6631–6637.

Dufrêne, Y. F., Marchal, T. G., & Rouxhet, P. G. (1999). Probing the organization of adsorbed protein layers: Complementarity of atomic force microscopy, X-ray photoelectron spectroscopy and radiolabeling. *Applied Surface Science*, *144–145*, 638–643.

Jo, T. A., Petri, D. F. S., Beltramini, L. M., Lucyszyn, N., & Sierakowski, M.-R. (2010). Xyloglucan nano-aggregates: Physico-chemical characterization in buffer solution and potential application as a carrier for camptothecin. *Carbohydrate Polymers*, *82*, 355–362.

Haddon, R. C., & Lamola, A. A. (1985). The molecular electronic device and the biochip computer: Present status. *Proceedings of the National Academy of Sciences*, *82*(27), 1874–1878.

Hauck, T. S., Giri, S., Gao, Y., & Chan, W. C. W. (2010). Nanotechnology diagnostics for infectious diseases prevalent in developing countries. *Advanced Drug Delivery Reviews*, *62*(4–5), 438–448.

Hayashi, T. (1989). Xyloglucans in the primary cell wall. *Annual Review of Plant Physiology*, *40*, 139–168.

Hirose, M., Yasaka, T., Takakura, M., & Miyazaki, S. (1991). Initial oxidation of chemically cleaned silicon surfaces. *Solid State Technology*, *34*, 43–48.

Leung, B. O., Hitchcock, A. P., Cornelius, R., Brash, J. L., Scholl, A., & Doran, A. (2009). X-ray spectromicroscopy study of protein adsorption to a polystyrene–polylactide blend. *Biomacromolecules*, *10*(7), 1838–1845.

Liu, Z. H., & Brown, N. M. D. (1998). XPS characterization of mica surfaces processed using a radio-frequency (rf) argon plasma. *Journal of Physics D: Applied Physics*, *31*, 1771–1781.

Lucyszyn, N., Lubambo, A. F., Ono, L., Jó, T. A., Souza, C. F., & Sierakowski, M.-R. (2011). Chemical, physico-chemical and cytotoxicity characterisation of xyloglucan from *Guibourtia hymenifolia* (Moric.) J. Leonard seeds. *Food Hydrocolloids*, *25*, 1242–1250.

Lubambo, A. F., Lucyszyn, N., Klein, J. J., Schreiner, W. H., de Camargo, P. C., & Sierakowski, M.-R. (2009). Dewetting pattern and stability of thin xyloglucan films adsorbed on silicon and mica. *Colloids and Surfaces B: Biointerfaces*, *70*, 174–180.

Lubambo, A. F., Lucyszyn, N., Petzhold, C. L., de Camargo, P. C., Sierakowski, M.-R., Schreiner, W. H., et al. (2011). Self-assembled polystyrene/xyloglucan nanospheres from spin coating evaporating mixtures. *Carbohydrate polymers*, *84*(1), 126–132.

Miyazaki, S., Suisha, F., Kawasaki, N., Shirakawa, M., Yamatoya, K., & Attwood, D. (1998). Thermally reversible xyloglucan gels as vehicles for rectal drug delivery. *Journal of Controlled Release*, *56*, 75–83.

Miyazaki, S., Kawasaki, N., Kubo, W., Endo, K., & Attwood, D. (2001). Comparison of *in situ* gelling formulations for the oral delivery of cimetidine. *International Journal of Pharmaceutics*, *220*(1–2), 161–168.

Powell, T. B., Tran, P. L., Kim, K., & Yoon, J.-Y. (2009). Size-dependent self-assembly of submicron/nano beads-protein conjugates for construction of a protein nanoarray. *Journal of Materials Science and Engineering C*, *29*(8), 2459–2463.

Rusmini, F., Zhong, Z., & Feijen, J. (2007). Protein immobilization strategies for protein biochips. *Biomacromolecules*, *8*(6), 1775–1789.

Priestley, R. D., Ellison, C. J., Broadbelt, L. J., & Torkelson, J. M. (2005). Structural relaxation of polymer glasses at surfaces, interfaces, and in between. *Science*, *309*, 4456–4459.

Sordi, M. L. T., Riegel, I. C., Ceschi, M. A., Müller, A. H. E., & Petzhold, C. L. (2010). Synthesis of block copolymers based on poly(2,3-epithiopropylmethacrylate) via RAFT polymerization and preliminary investigations on thin film formation. *European Polymer Journal*, *46*(2), 336–344.

Wadhwa, G. (1990). Biochips and biocomputers—future of computing and medicine. *Journal of Scientific & Industrial Research*, *49*, 486–491.

Zhao, Y., & Marshall, J. S. (2008). Spin coating of a colloidal suspension. *Physics of Fluids*, *20*(4), 043302-1–043302-15.